View metadata, citation and similar papers at core.ac.uk
brought to you by CORE
provided by Infoscience - École polytechnique fédérale de Lausanne

Resonant-Body Silicon Nanowire Field Effect Transistor without Junctions

Sebastian T. Bartsch,[1] Cécilia Dupré,[2] Eric Ollier,[2] Adrian M. Ionescu[1]

[1] Nanoelectronic Devices Laboratory, Ecole Polytechnique Fédéral de Lausanne (EPFL), 1015 Lausanne, Switzerland
phone: +41 21 693 3978 fax: +41 21 693 3640 email: adrian.ionescu@epfl.ch
[2] CEA, LETI, MINATEC Campus, 38054 Grenoble Cedex 9, France.

Abstract

We demonstrate the first implementation of a highly doped, silicon nanowire electromechanical resonator that exploits the depletion charge modulation in a junctionless FET to transduce mechanical motion on-chip. The resonator, with a typical length between 1 and 2 µm, a total height of 45 nm and a total width of 65 nm, is coupled *via* two lateral 60 nm air-gap gate electrodes. A fundamental resonance frequency of up to 226 MHz is detected in the drain current. This device is integrated in an FD-SOI-CMOS platform using conventional 8" inch wafer technology, which offers unique opportunities for compact sensing platforms interfaced with CMOS on a single chip.

Introduction

In the past decade, nanoelectromechanical systems (NEMS) have been continuously proposed for the ultra-sensitive detection of small mass and force [1]. A major challenge towards practical sensor systems based on sub-100 nm NEMS is their large-scale integration, actuation and read-out on-chip. Piezoresistance in silicon has been successfully harnessed in nanowire resonators at very high operating frequencies [2]. Merging FETs with NEMS have recently demonstrated enhanced performance, owing to their intrinsic tunable gain and record-low power consumption levels [3]. In this study, we implemented a double-gate junctionless FET into a nanowire electromechanical resonator. We demonstrate that the FET gain can be harnessed to transduce mechanical motion of *ultra-thin* silicon resonators at very high frequencies.

A Resonant-Body Transistor without Junctions

A. Principle

Junctionless FETs have been proposed by Colinge *et al.* [4] in order to address the scaling challenges of nanowire transistors. Such devices are highly doped and the ON-state is characterized by a conduction channel in the entire silicon body; by applying a gate bias, the conduction channel can be depleted, and eventually pinch-off the conduction path (OFF-state). In the static regime, the drain current in a junctionless transistor consisting of a highly n-doped nanowire body with lateral gates is given by:

$$I_D = q\mu N_D \frac{t_{Si}(W_{Si} - 2W_{dep}(V_G))}{L} V_D \qquad (1)$$

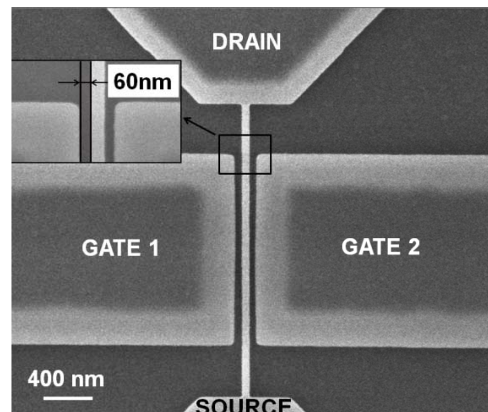

Fig. 1. SEM image of a 2.3 µm long, 65 nm wide and 45 nm thick nanowire resonator. Electromechanical coupling is achieved through ~ 60 nm flexible air-gap capacitors. The nanowire resonates in-plane.

where W_{Si} is the body (lateral) width, N_D the channel doping concentration, t_{Si} the channel thickness and L the channel lengths. Here, the gate voltage controls the depletion width W_{dep}, which varies at resonance. This is in total contrasts with the previously reported resonant body and resonant gate FET [3, 5-7], where the carrier density in inversion or accumulation layers was modulated to create a low resistivity path in a high resistivity channel region. The electromechanical (small signal) drain current is according to:

$$i_{FET} = \partial I_D \approx g_m(\tilde{v}_g + \frac{C'_{eq}}{C_{eq}} \cdot \tilde{z} \cdot V_G) \qquad (2)$$

where C_{eq} is the equivalent gate capacitance, C'_{eq} its derivative

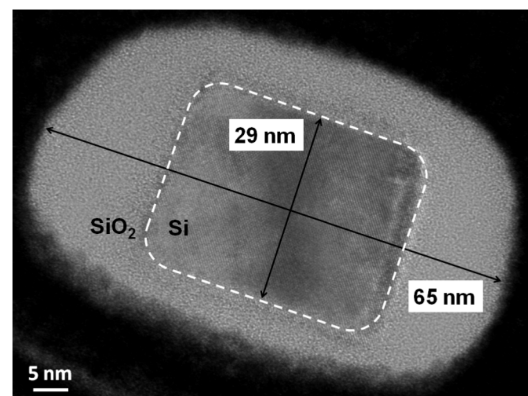

Fig. 2. Cross-sectional TEM image, with the silicon body indicated as dashed, white line. The (lateral) width of the silicon body is W_{Si} = 35 nm, the total (lateral) beam width is W_{beam} = 65 nm.

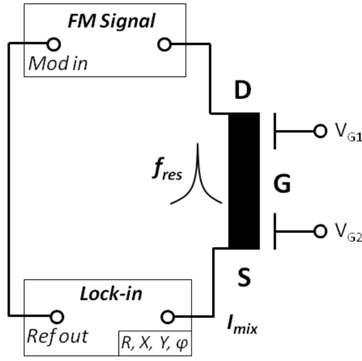

Fig. 3. Schematic of the signal routing used for the measurement of the resonant characteristics. The device is indicated as 4-terminal device, with drain (D), source (S) and two independent gate electrodes (G). The FM carrier drives the beam into motion. At resonance, the device demodulates the FM signal to yield a low-frequency signal I_{mix} (< 100 kHz) that can be detected *via* lock-in amplification. The quadratures X and Y of I_{mix} are recorded as function of the swept frequency.

with respect to the nanowire position, $\tilde{v}_g$ the a.c. voltage and $\tilde{z}$ the (time-varying) motion of the nanowire. The key to fabricating junctionless resonant-body FETs is to form a suspended, crystalline silicon structure that is sufficiently thin to fully deplete the transistor channel via the action of the nearby gate electrode. Therefore, the transduction principle proposed here is suited solely for a class of ultra-thin silicon resonators, and principally not limited by further dimensional scaling.

B. Fabrication and Characterization

We used a 40 nm thin device layer on 8" inch SOI wafers to fabricate NEMS based on a typical SOI-release process. Two ion implantations with boron (p+) and phosphorus (n+), define the gate (> 1×10^{20} cm^{-3}) and the channel doping concentration (~ 2×10^{18} cm^{-3}), respectively. The device active area was

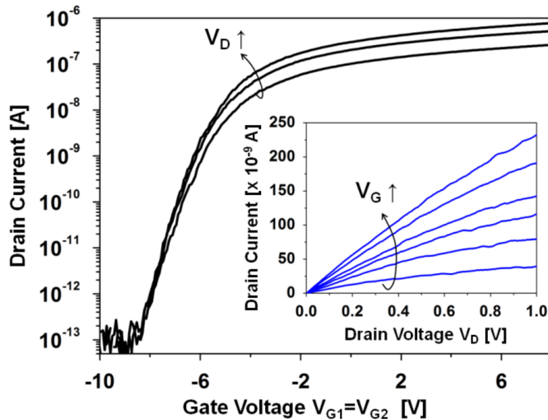

Fig. 4. The drain current vs. the (symmetric) gate voltage ($V_G = V_{G1} = V_{G2}$), for drain voltages V_D = 0.1V, 0.2V and 0.3V. The transfer curve shows off-currents corresponding to the detection limits of the measurement system (fA). **Inset**: Output characteristics, with drain current vs. drain voltage for different (symmetric) gate voltages V_G (from -5 V to -3.75 V, in steps of 0.25 V).

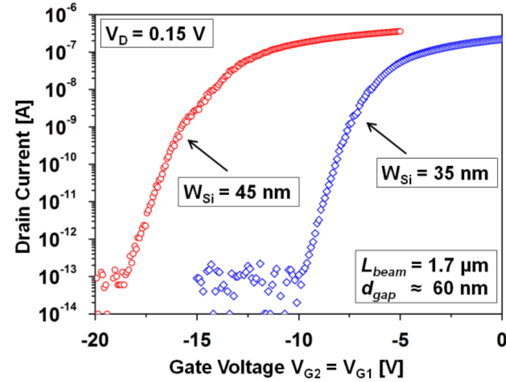

Fig. 5. The transfer characteristics I_D-V_G for two beams with different silicon body widths W_{si}.

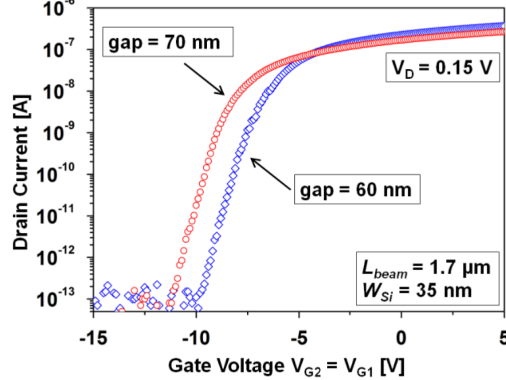

Fig. 6. The transfer characteristics I_D-V_G for two beams with the same W_{si}, but different gap design.

patterned via hybrid DUV/e-beam lithography. After release, the nanowire resonators were terminated with a 12 nm thermal

oxide, which ensures a low leakage current and improves electromechanical coupling. Fig. 1 shows the top-view, and Fig. 2 the cross-sectional view, respectively, of a representative device. Fabrication details and the actual co-integration with CMOS are described elsewhere [8]. The resonant, mechanical properties were investigated by exploiting the device as intrinsic signal mixer and FM

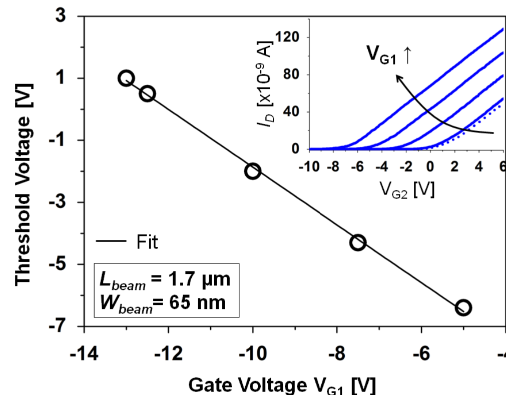

Fig. 7. The fine tuning of the threshold voltage *via* the "back-gate" voltage V_{G1}. The inset shows the according transfer curves I_D-V_{G2}, with V_{G1} as parameter.

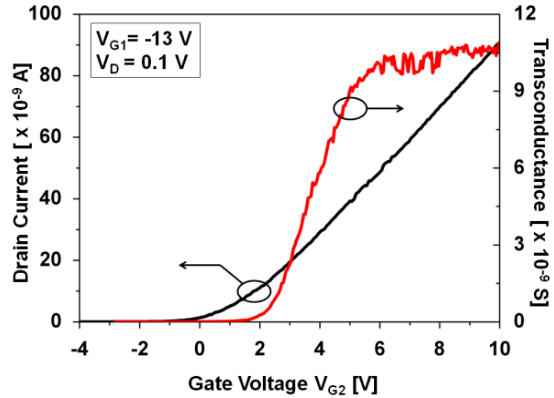

Fig. 8. The transfer curve I_D-V_{G2}, shown for asymmetric gate bias conditions, while V_{G1} is used as "back-gate" voltage and set constant at -13V and. The right axis shows the respective transconductance. These bias conditions were applied to detect the mechanical resonance.

demodulator. The setup is shown in Fig. 3, further details about his detection method can be found in Ref. [9]. All measurements were performed in a Süss Microtech vacuum probe chamber (<10^{-5} mbar) and at room temperature (300 K).

C. Static properties

The current-voltage characteristics revealed a well-behaved transition from the OFF- to the ON-state. The transfer curve (Fig. 4) showed on/off current ratios beyond 10^6 and clear exponential dependence in sub-threshold. The inset of Fig.4 shows the output characteristics I_D-V_D, indicating the linear operating region and the transition to current saturation at higher drain voltages ($V_D \approx$ 1V). Fig. 5 and Fig. 6 show the impact of different resonator designs on the transfer characteristics. For thinner beams, full depletion (OFF-state) is achieved at higher gate voltages. On the other hand, a larger

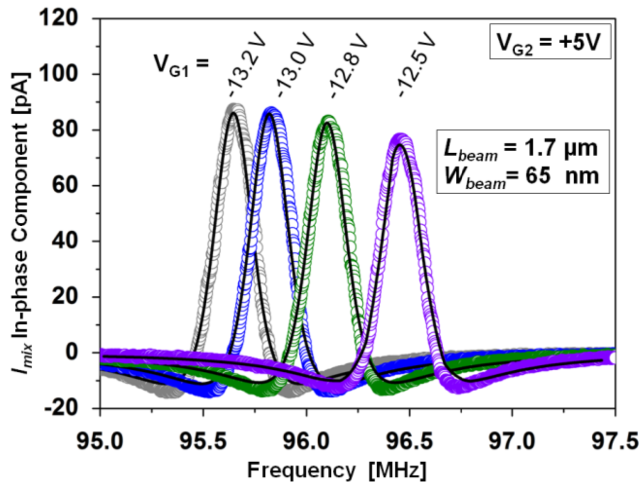

Fig. 9. Fundamental mechanical resonance at 96 MHz. The detected drain current I_{mix} is plotted vs. frequency. The resonance can be tuned by varying the gate voltage V_{G1}, with the values -13.2 V, -13.0 V, -12.8 V and -12.5 V. The FM parameters were chosen at f_m = 2 kHz and Δf = 75 kHz (f_m is the frequency of modulation and Δf the frequency deviation). The input drive power is set at -34 dBm.

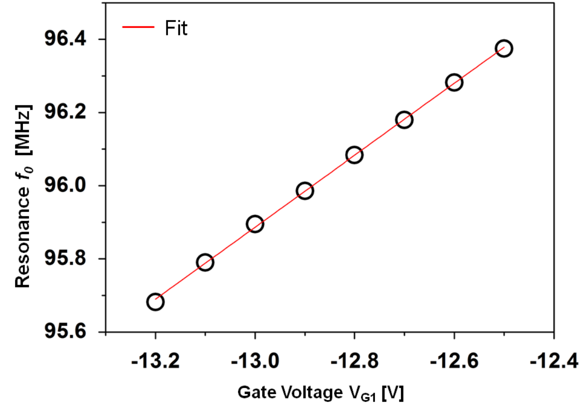

Fig. 10. The resonance frequency is shown vs. the d.c. gate bias V_{G1}. Due to the electrostatic actuation, the effective spring constant is lowered with increasing d.c. voltage. This leads to a reduction of the resonance frequency. The tunability is $df_0/dV_G \approx$ 0.96 MHz/V.

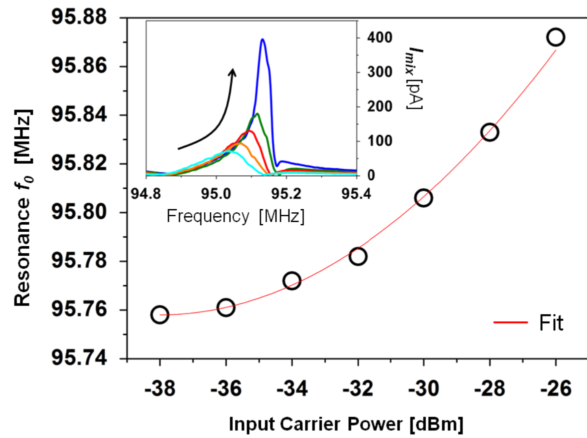

Fig. 11. The resonance frequency is shown as a function of the drive power. The increase in frequency is typical for a Duffing oscillator and indicates the presence of a mechanical nonlinearities (see inset).

air-gap results in an increase in threshold voltage (Fig. 6). Fig. 7 highlights the tunability of the threshold voltage in this device architecture, thanks to the two independent gate electrodes V_{G1} and V_{G2} (V_{G1} is set as parameter).

D. Resonant properties

For resonant operation, the FET was biased around threshold voltage (i.e., at max. transconductance), but with asymmetric gate bias (V_{G1}= -13V; V_{G2}= +5V, see Fig. 8). The drain current path was thereby concentrated on the outer edge of the silicon body, where the strongest current modulation, and hence mechanical displacement gain, can be expected, induced by the beam's motion. Fig. 9 shows the mechanical amplitude spectrum of a junctionless resonant-body nanowire FET with a length of 1.7 µm and fundamental resonance at 96 MHz, plotted for different gate voltages of V_{G1}. In this work, the in-phase component X of I_{mix} was chosen to represent the resonant characteristics, yielding the most accurate fit (black solid lines). Note that $X \sim R \cos \Phi$, which can assume negative value, and accounts for the negative sign of I_{mix} in Fig. 9 and

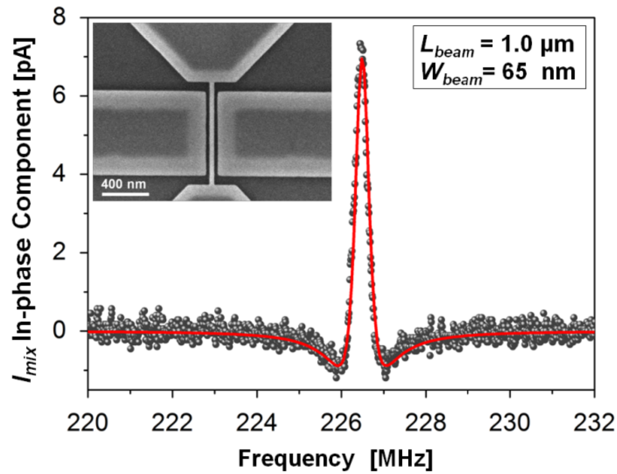

Fig. 12. The detected drain current versus the frequency of a nanowire with a length of 1 µm. The fundamental mechanical resonance at 226.49 MHz has a quality factor of ~250. The device is biased at V_{G1}= -20 V, V_{G2}= +5 V with an input power of -30 dBm. The inset shows the SEM image of the DUT.

Fig. 12 (Φ is the relative phase between the detected signal and its lock-in reference, and $R=\sqrt{X^2+Y^2}$ is the absolute magnitude of the detected signal). The extracted quality factors were in the order Q = 400-500. The tuning of the resonance frequency as function of the gate d.c. bias in Fig. 10. The spring softening effect due to the electrostatic actuation leads to a reduction of the resonance frequency. We obtained a considerable tunability of $df_0/dV_G \approx$ 0.96 MHz and a tuning range beyond 5%. With increasing input drive strength, the typical response of Duffing resonator can be observed (Fig. 11). This leads to a increase in resonance frequency, with quadratic dependence on the input drive. Fig. 12 depicts the fundamental resonance at 226 MHz of a 1 µm long device, whose frequency is among the highest resonant frequencies measured with integrated silicon nanowire resonators to date. In an application as mass detector, the presented resonator (96 MHz) may offer limits of detection in the sub-ag range (*ag* - 10^{-18} g) in vacuum, given a mass responsivity of $\mathcal{R}$ ~ 32 Hz/zg (*zg* - 10^{-21} g) and a fractional frequency stability achievable in the ppm-range [2].

Conclusion

In this paper, we have demonstrated a self-aligned, junctionless *silicon nanowire electromechanical FET* with two lateral 60 nm air-gap gates. The depletion charge modulation can be harnessed to transduce mechanical resonance on-chip at very high frequencies and is suited for a class of very scaled (sub-50 nm) silicon NEMS. Interfaced with advanced CMOS, these devices could be used for complex collective electromechanical signal processing based on thousands of resonant transistors, embedded on a single silicon chip. The presented results should foster a wide range of applications in RF, analog and extreme mass sensing.

References

[1] Hanay, M.S. *et al.*, Single-protein nanomechanical mass spectrometry in real time, *Nat. Nanotechnol.*, *in press*, 2012.

[2] Feng, X.L., He, R.R., Yang, P.D. Roukes, M.L. Very high frequency silicon nanowire electromechanical resonators. *Nano Lett* 7, 1953-1959, 2007.

[3] Bartsch, S. T., Lovera, A., Grogg, D., Ionescu, A. M. Silicon nanomechanical resonators with intrinsic tunable gain and sub-nW power consumption. *Nano* 84, 1771-1773, 2004.

[4] Colinge, J.P., Lee, C.W., Afzalian, A., Akhavan, N.D., Yan, R. *et al.* Nanowire transistors without junctions. *Nat. Nanotechnol.* 5, 225-229, 2010.

[5] Grogg, D., Ionescu, A.M. The vibrating body transistor. *IEEE T Electron Dev* 58, 2113-2121, 2011.

[6] Abele, N., Fritschi, R., Boucart, K., Casset, F., Ancey, P. *et al.* Suspended-gate MOSFET: Bringing new MEMS functionality into solid-state MOS transistor. *International Electron Device Meeting IEDM*, 1075-1077, 2005.

[7] Weinstein, D. Bhave, S.A. The resonant body transistor. *Nano Lett* 10, 1234-1237, 2010.

[8] Ollier, E. *et al.*, *Proceedings of the IEEE International Conference on Micro Electro Mechanical Systems (MEMS)* , art. no. 6170421 , pp. 1368-1371, 2012.

[9] Bartsch, S.T., Rusu, A., Ionescu, A.M. Single Active Nanoelectromechanical Tuning Fork as Front-end Radio-frequency Receiver, *Nanotechnology* 23, 225501, 2012.

Acknowledgments: This work was partially supported by the European Framework Project FP7 NEMSIC.